

# The Galactic Centre star S2 as a dynamical probe for intermediate-mass black holes

A. Gualandris<sup>1\*</sup>, S. Gillessen<sup>2</sup> and D. Merritt<sup>3\*</sup>

<sup>1</sup>*Max-Planck Institut für Astrophysik, Karl-Schwarzschild-Str. 1, D-85748 Garching, Germany*

<sup>2</sup>*Max-Planck Institut für Extraterrestrische Physik, Giessenbach-Str., D-85748, Garching, Germany*

<sup>3</sup>*Department of Physics and Center for Computational Relativity and Gravitation, Rochester Institute of Technology, 54 Lomb Memorial Drive, Rochester, NY*

## ABSTRACT

We study the short-term effects of an intermediate mass black hole (IBH) on the orbit of star S2 (S02), the shortest-period star known to orbit the supermassive black hole (MBH) in the centre of the Milky Way. Near-infrared imaging and spectroscopic observations allow an accurate determination of the orbit of the star. Given S2’s short orbital period and large eccentricity, general relativity (GR) needs to be taken into account, and its effects are potentially measurable with current technology. We show that perturbations due to an IBH in orbit around the MBH can produce a shift in the apoapsis of S2 that is as large or even larger than the GR shift. An IBH will also induce changes in the plane of S2’s orbit at a level as large as one degree per period. We apply observational orbital fitting techniques to simulations of the S-cluster in the presence of an IBH and find that an IBH more massive than about  $1000 M_{\odot}$  at the distance of the S-stars will be detectable at the next periapse passage of S2, which will occur in 2018.

**Key words:** black hole physics – stellar dynamics – methods:  $N$ -body simulations – Galaxy: centre

## 1 INTRODUCTION

The innermost arcsecond of the Milky Way harbours a cluster of young massive stars (the S-star cluster) in eccentric orbits around the supermassive black hole (MBH). Near-infrared observations of the cluster allow a precise determination of the trajectories of about 20 stars. These can be used to derive fundamental parameters like the mass of the MBH and the distance to the Galactic centre, as well as to constrain the gravitational potential and test predictions from general relativity (GR) (Rubilar & Eckart 2001; Zucker et al. 2006). Since the collapse of a giant molecular cloud at the distance of the S-cluster is prevented by the tidal force of the MBH, it is believed that either the S-stars formed in-situ via a non-standard process or that they originated outside the black hole’s sphere of influence and then migrated to their current location. Among the in-situ models are the two disks model (Löckmann et al. 2009) and the eccentric instability model (Madigan et al. 2009). The two main models suggested for the transport of the stars are the cluster infall scenario (Gerhard 2001), also aided by an intermediate-mass black hole (IBH) (Hansen & Milosavljević 2003; Kim et al.

2004; Levin et al. 2005; Merritt et al. 2009; Fujii et al. 2009, 2010), and the binary disruption scenario (Gould & Quillen 2003; Perets et al. 2007, 2009). The properties and efficiency of these models are discussed in Perets & Gualandris (2010).

The star with the shortest orbital period ( $\sim 15$  yr), called S2 (Schödel et al. 2002; Ghez et al. 2003), has a semi-major axis  $a = (0.1246 \pm 0.0019)''$  and an eccentricity  $e = 0.8831 \pm 0.0034$  (Gillessen et al. 2009). Adopting a distance to the Galactic centre  $R_0 = 8.28$  kpc,  $a \sim 5.0018$  mpc, while the periapsis and apoapsis distances are, respectively,  $r_p = 0.585$  mpc,  $r_a = 9.419$  mpc. For this set of orbital elements, GR precession is measurable with current instrumentation on a time-scale of about 10 years (Gillessen et al. 2009).

The relativistic (prograde) advance of the periapse angle is given in the case of a non-rotating black hole by

$$\Delta\varpi = \frac{3\pi}{1-e^2} \frac{R_S}{a} = \frac{6\pi G}{c^2} \frac{M_{\text{MBH}}}{a(1-e^2)} \quad (1)$$

per radial period (Weinberg 1972), where  $R_S = 2GM_{\text{MBH}}/c^2$  is the Schwarzschild radius of the black hole. For the Galactic centre black hole,  $R_S \approx 4.1 \times 10^{-7}$  pc for an assumed mass of  $M_{\text{MBH}} = 4.3 \times 10^6 M_{\odot}$  (Gillessen et al. 2009). As a result of the orbit’s precession, there is a dis-

\* E-mail: alessiag@mpa-garching.mpg.de

placement in the star's apoapse position that is given by

$$\Delta r_a \approx a(1+e)\Delta\varpi \approx \frac{6\pi GM_{\text{MBH}}}{c^2(1-e)} \quad (2)$$

again per radial period; note that this expression is independent of the semi-major axis. As seen from Earth, this shift corresponds to an angle on the sky of

$$\Delta\Theta_a \sim 0.097 \text{ mas} \left( \frac{1}{1-e} \right) \left( \frac{M_{\text{MBH}}}{4.3 \times 10^6 M_\odot} \right) \left( \frac{8.28 \text{ kpc}}{R_0} \right) \quad (3)$$

which amounts to  $\sim 0.83$  mas for star S2.

A complicating factor is the likely presence of a distributed mass within S2's orbit, consisting of stars and stellar remnants. Assuming that the mass density follows  $r^{-\gamma}$ , with  $r$  the distance from the MBH, the advance, per radial period, of orbital periapse due to the distributed mass is

$$\Delta\varpi \approx 2\pi \frac{M_\star(a)}{M_{\text{MBH}}} \sqrt{1-e^2} F(\gamma) \quad (4)$$

in the retrograde sense; here  $M_\star(r)$  is the distributed mass enclosed within radius  $r$  and  $F = (3/2, 1)$  for  $\gamma = (0, 1)$  (e.g. Merritt et al. 2010). Setting  $F \approx 1$ , this implies, for S2, a shift on the sky of

$$\Delta\Theta_a \approx 0.69 \text{ mas} \left( \frac{10^3 M_\star(a)}{M_{\text{MBH}}} \right). \quad (5)$$

This is comparable with the relativistic precession if the distributed mass within S2's orbit is  $\gtrsim 10^{-3} M_{\text{MBH}}$ . Disentangling these two sources of precession will be difficult, requiring measurements of the radial velocity of S2 near periapse passage (e.g. Angéilil & Saha 2010).

Non-spherically-symmetric perturbations, if present, can affect not just the periapse angle but also the angular momentum of S2's orbit, resulting in changes in  $e$  and in the orientation of its orbital plane. Potentially the largest source of such perturbations is a second massive black hole orbiting somewhere near S2. In fact, the orbits of the S-stars are consistent with the long-term presence of an IBH in their midst, with mass  $\sim 10^3 M_\odot$  (Merritt et al. 2009; Gualandris & Merritt 2009). While an IBH would also contribute to the periapse advance of S2, its key signature would be a change in S2's orbital angular momentum.

In this work, we combine high-accuracy  $N$ -body simulations (§2) with orbital fitting techniques (§3) to investigate the observable effects of an IBH on the orbit of star S2 over a time-scale of a few orbital revolutions. In §4 we discuss the other types of perturbation that could potentially induce changes in S2's orbital angular momentum and compare them with perturbations from an IBH. §5 sums up.

## 2 INITIAL MODELS AND NUMERICAL METHODS

We consider  $N$ -body models that include a MBH, an IBH and the S-star cluster. The initial conditions for the stars are derived from the orbital elements given by Gillessen et al. (2009). For star S2, we take the improved elements from Gillessen et al. (2009). Of the 28 stars for which those authors provide orbital elements, we exclude the six stars (S66, S67, S83, S87, S96, S97) which likely belong to the clockwise disk (Genzel et al. 2003; Paumard et al. 2006) and star S111

which appears to be unbound. We are left with a sample of 21 stars with well defined orbits, for which we determined positions and velocities at 2008 AD from the classical elements. The masses of the S-stars were set to  $10 M_\odot$  (e.g. Eisenhauer et al. 2005) except for star S2 for which a value of  $20 M_\odot$  was adopted (Martins et al. 2008).

The IBH is placed on a Keplerian orbit around the MBH. We adopt four different values for the mass ratio of the black hole binary  $q \equiv M_{\text{MBH}}/M_{\text{IBH}} = (1.0 \times 10^{-4}, 2.5 \times 10^{-4}, 5.0 \times 10^{-4}, 1.0 \times 10^{-3})$ , five values for the semi-major axis  $a = (0.3, 1, 3, 10, 30)$  mpc, four values for the eccentricity  $e = (0, 0.5, 0.7, 0.9)$  and twelve choices for the direction of the orbit's angular momentum vector (the same set as in Gualandris & Merritt (2009)), for a total of 960 sets of initial conditions. The IBH begins from orbital periapsis in all cases. The initial value of the mean anomaly is likely to be unimportant in all cases for which the orbital period of the binary is much smaller than the integration time (50 yr), i.e.  $a = 0.3, 1, 3$  mpc. For  $a = 30$  mpc, only part of the IBH orbit is sampled by the integration, and in principle the choice of the initial position might have an effect on the interaction with S2. However, at a distance of 30 mpc the IBH is completely outside S2's orbit for  $e \lesssim 0.7$ , and there is essentially no detectable signature, as shown below. The only set of simulations for which the initial mean anomaly of the IBH might be important is the  $a = 10$  mpc, which corresponds to an orbital period of about 43 yr for the IBH. We perform an extra set of simulations for  $a = 10$  mpc starting the IBH at apoapsis rather than periapsis and we compare the results in the two cases.

We advanced each  $N$ -body system in time using the AR-CHAIN code (Mikkola & Merritt 2008), a recent implementation of the algorithmic regularisation method that is able to reproduce the motion of tight binaries for long periods of time with extremely high precision. The code combines the use of the chain structure, introduced originally by Mikkola & Aarseth (1993), with a new time transformation to avoid singularities and achieve high precision for arbitrary mass ratios. Note that we self-consistently follow not just the interactions of S2 with the MBH and IBH, but all other interactions as well, including star-star interactions. The integration interval was 50 years, during which time S2 performs three full orbits.

The AR-CHAIN code includes relativistic corrections to the accelerations up to 2.5 post-Newtonian order for all interactions involving the MBH particle. General relativistic advance of the periapse, which operates on a time-scale

$$\begin{aligned} T_\varpi &\equiv \left| \frac{\Delta\varpi}{2\pi P} \right|^{-1} = \frac{2\pi c^2 (1-e^2) a^{5/2}}{3(GM_{\text{MBH}})^{3/2}} \\ &\approx 1.3 \times 10^5 \text{ yr} \left( \frac{a}{5 \text{ mpc}} \right)^{5/2} \left( \frac{4.3 \times 10^6 M_\odot}{M_{\text{MBH}}} \right)^{3/2} (1 - \epsilon^2) \end{aligned} \quad (6)$$

is accounted for by the 1PN and 2PN terms. The dissipative term arising from the emission of gravitational waves is accounted for by the 2.5PN term; this term is potentially important for the IBH, for which the associated coalescence

time-scale is

$$T_{\text{GW}} = \frac{5}{256F(e)} \frac{c^5}{G^3} \frac{a^4}{\mu (M_{\text{MBH}} + M_{\text{IBH}})^2}$$

$$\approx \frac{1.96 \times 10^{13} \text{ yr}}{F(e)} \left( \frac{a}{5 \text{ mpc}} \right)^4 \left( \frac{4.3 \times 10^6 M_{\odot}}{M_{\text{MBH}}} \right) \left( \frac{10^3 M_{\odot}}{M_{\text{IBH}}} \right)$$

$$\times \left( \frac{4.3 \times 10^6 M_{\odot}}{M_{\text{MBH}} + M_{\text{IBH}}} \right)$$

where

$$F(e) = (1 - e^2)^{-7/2} \left( 1 + \frac{73}{24} e^2 + \frac{37}{96} e^4 \right)$$

and

$$\mu = \frac{M_{\text{MBH}} M_{\text{IBH}}}{M_{\text{MBH}} + M_{\text{IBH}}} \approx M_{\text{IBH}}$$

is the reduced mass of the IBH/MBH binary. The orbital decay time-scale for the black hole binary is shown in Figure 1 for the two extreme values of the mass ratio and the four adopted values of the initial eccentricity. This time-scale is always much longer than our integration interval of  $\sim 50$  yr. In addition, it is longer than the main-sequence lifetime ( $\sim 10^7$  yr) of a 20 solar mass star for all initial configurations excepting the cases  $a = 0.3 \text{ mpc}$  and  $e \geq 0.7$ . In the former runs, it is justified to associate our initial parameters for the IBH/MBH binary with the parameters at some much earlier time, e.g. the epoch preceding formation of the S-stars. In the latter runs, the orbit of the IBH at some much earlier time would have been larger and/or more eccentric. The maximum relative variation of the binary semi-major axis in the  $N$ -body integrations is  $\Delta a/a \sim 10^{-3}$  while the absolute variation of the eccentricity is  $\Delta e \sim 10^{-2}$ .

### 3 IBH PERTURBATIONS

In the Schwarzschild metric, the argument of periape  $\varpi$  evolves due to in-plane precession. The two remaining angles that define the orientation of the orbit,  $i$ , the inclination, and  $\Omega$ , the position angle of the ascending node, are fully conserved in the relativistic two-body problem.<sup>1</sup> The semi-major axis and eccentricity are conserved at the IPN level, and we expect very small deviations due to higher order PN corrections in the integrations (Soffel 1989). In the limit of small star-to-black hole mass ratio, the semi-major axis and eccentricity in the PN approximation are given by (Soffel 1989)

$$a = \frac{-GM}{2\mathcal{E}} \left[ 1 + \frac{7}{2} \frac{\mathcal{E}}{c^2} \right] \quad (8)$$

$$e = \sqrt{1 + \frac{2\mathcal{E}}{G^2 M^2} \left( 1 + \frac{17}{2} \frac{\mathcal{E}}{c^2} \right) \left( \mathcal{J}^2 + 2 \frac{G^2 M^2}{c^2} \right)} \quad (9)$$

where

$$\mathcal{E} = \frac{1}{2} v^2 - \frac{GM}{r} + \frac{3}{8} \frac{v^4}{c^2} + \frac{GM}{2rc^2} \left[ 3v^2 + \frac{GM}{r} \right] \quad (10)$$

<sup>1</sup> We follow the standard practise of using the plane of the sky as the reference plane for defining  $(\Omega, i)$ .

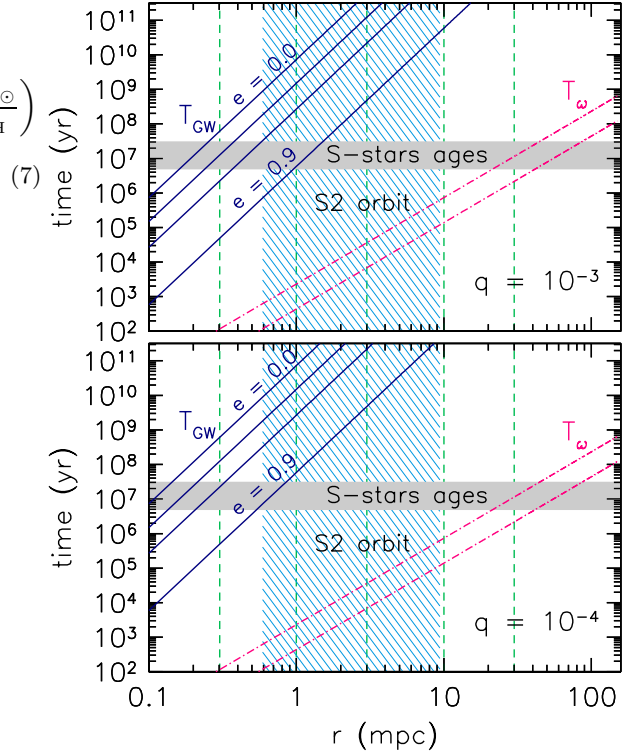


**Figure 1.** Time-scales associated with orbital evolution in our models. Solid lines show the GW time-scale, Eq. (7), for a black hole binary with  $q = 10^{-4}$  (top) and  $q = 10^{-3}$  (bottom), for four different values of the eccentricity  $e = 0, 0.5, 0.7, 0.9$ . Dashed-dotted lines show the GR precession time-scale for two different values of the eccentricity:  $e = 0$  (upper line) and  $e = 0.9$  (lower line). The vertical dotted lines represent the adopted values for the binary initial semi-major axis. The filled grey region indicates the estimated ages of the S-stars while the striped area shows the radial range of S2's orbit.

is the specific post-Newtonian energy and

$$\mathcal{J} = |\vec{x} \times \vec{v}| \left[ 1 + \frac{1}{2} \frac{v^2}{c^2} + \frac{3GM}{rc^2} \right] \quad (11)$$

the specific angular momentum. Here,  $\vec{x}$  and  $\vec{v}$  are the relative position and velocity vectors between the star and the MBH,  $M$  is the total mass, and  $c$  is the speed of light.

The presence of the other S-stars introduces small deviations from spherical symmetry in the gravitational potential but the effect on the orbital elements over these short time-scales is negligible, as we show in Section 5. Therefore, the variations that we observe in the orbital elements of star S2 in our simulations, namely the semi-major axis, eccentricity, inclination, and position angle of the ascending node, can be attributed to perturbations from the IBH.

Figure 2 summarises the changes in the orbital elements of S2 found in the  $N$ -body integrations. Plotted are the variations over one revolution averaged over the twelve different orientations of the initial IBH/MBH orbit. The dotted lines in the periaapsis and apoapsis panels indicate the variations due to GR. The shift in the periape corresponds to an observable angle  $\Delta\theta_p = \Delta\theta_a (1 - e) / (1 + e)$ , where  $\Delta\theta_a$  is

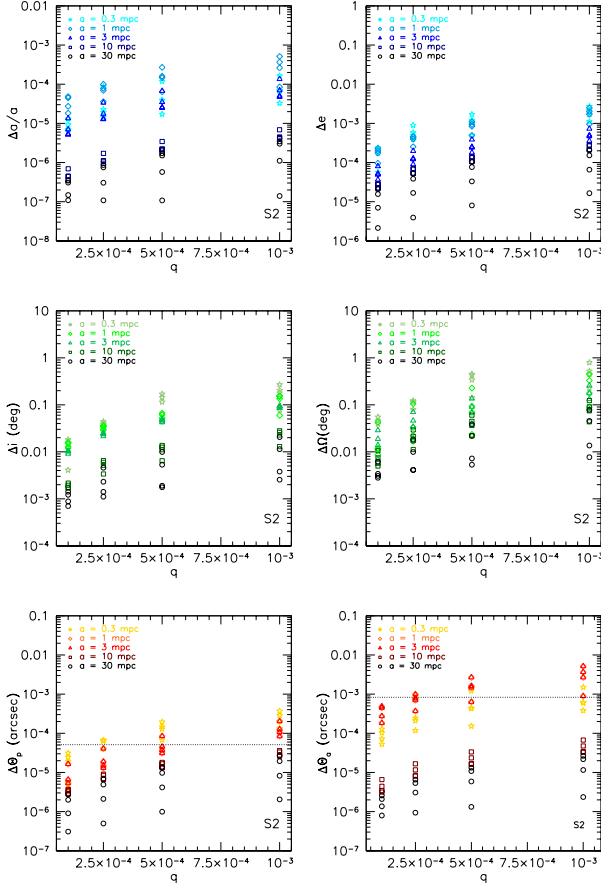


**Figure 2.** Average changes in the orbital elements (semi-major axis, eccentricity, inclination, position angle of the ascending node, periastron and apoastron) of star S2 over one full orbit, versus the mass ratio of the black hole binary. Different symbols are for different initial semi-major axes of the binary. Each point is an average over the 12 orientations of the IBH/MBH orbital angular momentum vector. The dotted lines represent the GR shift in the periastron and apoastron.

defined in Eq. 3. Note that the variations in the inclination  $i$  and position angle  $\Omega$  of the ascending node reach values close to 1 degree for the most massive IBHs considered. This is of the same order as the current observational accuracy ( $\sim 0.7$  deg). In 50 years, this value will drop to about 0.4 deg, assuming there are no technological improvements.

While precession induced by the PN terms is restricted to the orbital plane, an IBH induces more general changes in the orbital elements, including changes in the direction of the orbital angular momentum vector. We measure the latter via the angle

$$\cos \phi = \left( \frac{\vec{L}_i \cdot \vec{L}_f}{L_i L_f} \right). \quad (12)$$

Figure 3 plots  $\phi$  for all the runs, after averaging over the 12 different IBH orientations.

The changes in the orbital plane of S2 are larger for more massive IBHs and can reach values of  $\sim 1$  degree for  $q = 10^{-3}$ . Out-of-plane motion is also affected by the size

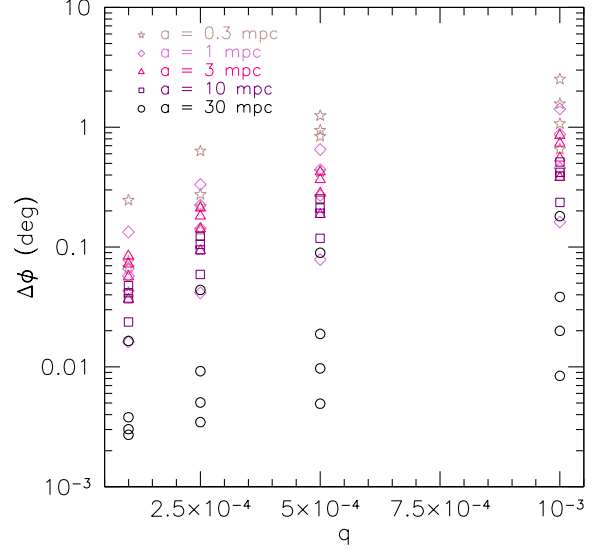


**Figure 3.** Mean variation of the orbital plane of star S2 as a function of the binary mass ratio. For each combination of binary mass ratio, semi-major axis and eccentricity, the results are averaged over the 12 orbital orientations of the IBH.

of the MBH/IBH binary orbit such that changes are largest for  $a \lesssim 10$  mpc.

The three-body system composed of MBH, IBH and S2 is reminiscent of a Kozai triple (Kozai 1962). However, the changes that we observe in the orbital elements are not generally attributable to the Kozai mechanism. Kozai oscillations can be induced if (i) the MBH - S2 - IBH system can be regarded as a hierarchical triple, with well-separated orbital periods for the inner and outer orbit; (ii) the period predicted for the Kozai oscillations is shorter than that of any other precessional period, in this case, GR precession; (iii) the outer orbit is largely inclined with respect to the inner orbit. The first condition is only satisfied in the runs with  $a = 10, 30$  mpc.

The timescale for Kozai oscillations can be written as (Kinoshita & Nakai 2007)

$$T_K = \frac{4\mathcal{K}}{3\sqrt{6}\pi} \frac{P_{\text{out}}^2}{P_{\text{inn}}} \frac{M_{\text{MBH}} + m_*}{M_{\text{IBH}}} (1 - e_{\text{out}}^2)^{3/2} \quad (13)$$

where  $P_{\text{inn}}$  and  $P_{\text{out}}$  are the period of the inner and outer binary,  $e_{\text{out}}$  is the eccentricity of the outer orbit and  $\mathcal{K}$  is a numerical coefficient which depends only on the initial values of the relative inclination angle  $\alpha$ , the inner binary eccentricity  $e_{\text{inn}}$  and the inner binary argument of periastron  $\varpi$ . The maximum eccentricity  $e_{\text{max}}$  attained by the inner binary is also a function of the initial values of  $\alpha$ ,  $e_{\text{inn}}$  and  $\varpi$  only. Figure 4 shows  $T_K$  as a function of the black hole binary mass ratio for the assumed values of the eccentricity and for two allowed separations. We find that  $T_K$  is always longer than S2's GR precession timescale of  $2.5 \times 10^4$  yr for  $a = 30$  mpc. For the remaining case  $a = 10$  mpc,  $T_K$  is short enough only for  $q \gtrsim 2.5 \times 10^{-4}$  and  $e \gtrsim 0.7$ . This restricts the applicability of the Kozai mechanism to a small subset of our simulations, in contrast with the results shown in Figure 2 and in the following section. We conclude that the Kozai

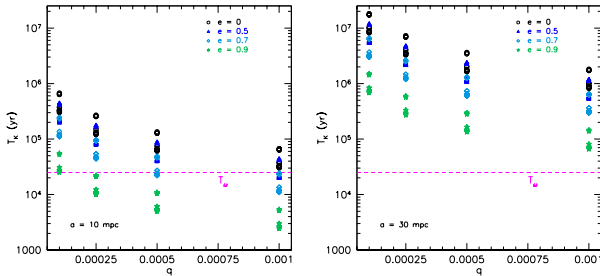


**Figure 4.** Timescale for Kozai oscillations in star S2 as a function of the black hole binary mass ratio for different values of the binary eccentricity. The left panel refers to simulations with  $a = 10$  mpc while the right panel is for  $a = 30$  mpc. The horizontal lines marks the GR precession timescale for S2.

mechanism is not the dominant effect producing changes in orbital  $e$  and  $i$  in our simulations. In those cases where it is potentially relevant, the eccentricity is predicted to oscillate between  $e_{\min} = 0.24 - 0.74$  and  $e_{\max} = 0.89 - 0.99$  over one Kozai period, depending on the values of  $\alpha$  and  $\varpi$ . This implies variations of the order of  $2 \times 10^{-5} - 6 \times 10^{-3}$  over the integration time of 50 years (for  $a = 10$  mpc).

The apoapsis shift due to perturbations from the IBH is very sensitive to the binary parameters. In the case of  $q \gtrsim 5 \times 10^{-4}$  and  $a \lesssim 3$  mpc, the shift over one revolution due to the IBH becomes larger than the relativistic shift. This suggests a variation in the orbital elements which is potentially observable with current instrumentation.

However, the observability of variations in the orbit of S2 depends on several factors. In the following section we thoroughly examine all such factors and use orbital fitting to determine whether an IBH is detectable via on-going monitoring of the S-cluster. Theoretically, it would be possible to use other S-stars to investigate the effects of a hypothetical IBH. Given that the shifts in the apparent location of periastris and apoapsis depend only on the eccentricity and not on the semi-major axis of the stellar orbit, it would seem appropriate to consider all stars with  $e \gtrsim 0.8$  for such an analysis. From an observational point of view, however, S2 is the only star in the sample which is bright enough and not affected by confusion to allow for meaningful tests of the gravitational potential. We therefore limit our study to star S2.

## 4 ORBITAL FITTING

In this section we extract observational-like data from the simulated orbital traces of S2. We assume that eight or nine astrometric epochs can be obtained each year over the course of 50 years. The eight or nine yearly epochs are not evenly distributed but are spread over seven months only, thus taking into account the fact that the Galactic Centre is accessible with NIR observations only for part of the year. At the chosen epochs, the original, simulated positions are perturbed by an astrometric error, assumed to be distributed in a Gaussian fashion. We use a value of  $300 \mu\text{as}$  per coordinate, which is a conservative assumption for S2 (Fritz et al. 2010). The statistical uncertainty of the measured S2 posi-

tions is smaller than the assumed value. However, unrecognised confusion events with fainter stars are an additional, important error source, such that we consider our value realistic. Furthermore, we assume that the radial velocity of S2 is determined at two epochs per year. Here, we adopt a Gaussian error of  $15 \text{ km s}^{-1}$ . This value is typically reached with current NIR medium-resolution spectrographs.

In this way we obtain 960 simulated data sets that are reasonably close to what one would obtain by simply continuing the monitoring of orbits in the Galactic Centre with existing instruments. The fact that within the next 50 years new facilities with improved angular resolution will become available (such as the NIR interferometers ASTRA (Pott et al. 2008) and GRAVITY (Eisenhauer et al. 2005), or the extremely large telescopes TMT and E-ELT) means that an IBH probably will be detectable more easily than what we derive here. There is a second reason why we consider our procedure conservative. Observers may adopt a sampling strategy for the orbits other than a simple constant rate, as we assume here. Given the fact that the most constraining part of an orbit is the periastris passage, and the event is predictable, an intensification of the observations around the periastris passage provides an improved sampling pattern.

We fit each of the 960 data sets with the same code as used in Gillessen et al. (2009). From the fits, we determine the full set of 13 parameters describing the orbits and the potential: The six orbital elements ( $a, e, i, \Omega, \varpi, t_P$ ) and seven parameters describing the gravitational potential of the MBH: Mass, distance, on-sky position (2 parameters) and velocity (3 parameters) of the MBH. While in the simulations these quantities are known, this is not the case when the data sets are considered as mock observations. Then these quantities have to be treated as free fit parameters, since they need to be determined from the same orbital data from which the presence of an IBH shall be judged. Currently, nearly all constraints on these parameters actually come from the S2-orbit which we consider here. In future, some of the parameters describing the MBH might be determined independently from the orbit of other S-stars. We neglect this here and keep all seven parameters completely free. This is conservative, because additional constraints would make the presence of an IBH more easily detectable.

Using a purely Keplerian point-mass model is inadequate for all our data sets. The relativistic precession is too large during the 50 years of evolution and therefore we include the first order PN correction to the equations of motion when fitting the orbits (Gillessen et al. 2009). For example, all twelve data sets with  $(q = 1.0 \times 10^{-3}, a = 30 \text{ mpc}, e = 0.9)$  are well fit by the relativistic equations. In contrast, none of these data sets can be described by a purely Keplerian point-mass potential. Still, the relativistic potential only yields a perfect fit for some of the data sets. For others, the IBH perturbs the dynamics too strongly, and would therefore be detectable. Given that our sampling in radial velocity is rather sparse, the inclusion of special relativistic corrections to the radial velocities is not needed.

Note that it is not legitimate to assess the goodness of a fit by comparing the obtained parameters with those used as input for the simulations. Instead, we use the reduced  $\chi^2$  for each of the 960 fits to decide whether a fit is acceptable or not. We obtain values between 0.88 and 357. In addition, we

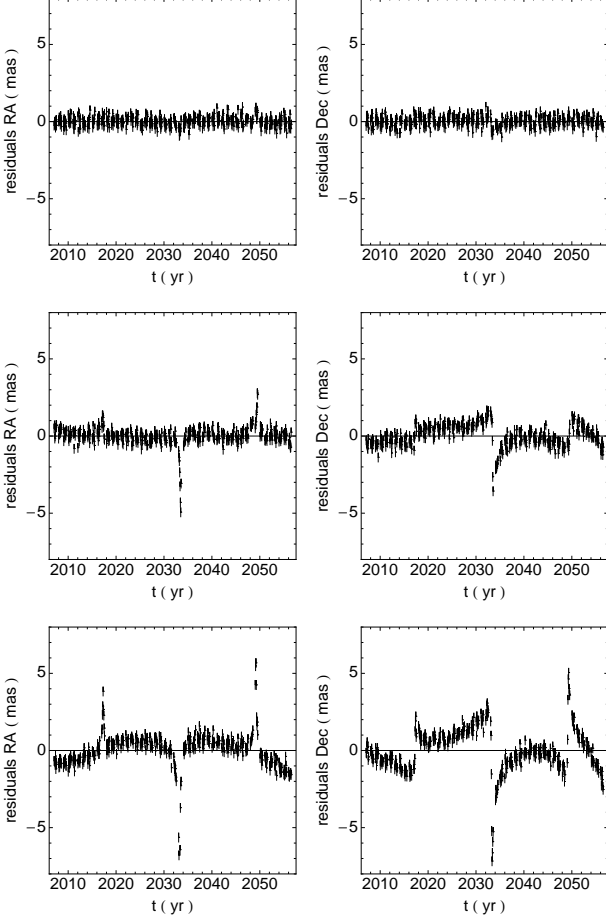


**Figure 5.** Examples of fit residuals. Top row: A fit using a simulated data set with ( $q = 1.0 \times 10^{-4}$ ,  $a = 3$  mpc,  $e = 0$ ). Middle row: a fit with ( $q = 2.5 \times 10^{-4}$ ,  $a = 0.3$  mpc,  $e = 0.9$ ). Bottom row: a fit with ( $q = 5 \times 10^{-4}$ ,  $a = 1$  mpc,  $e = 0$ ). The first (top) one is classified as acceptable and has a reduced  $\chi^2 = 1.15$ . The other two are classified as not acceptable and have reduced  $\chi^2$  values of 4.4 and 22.7 respectively.

examine the residuals of each fit by eye, dividing them into two categories: A set of fits for which the residuals do not visually show obvious correlations and a set for which it is apparent that the chosen gravitational potential model is not adequate. Figure 5 shows typical examples of the residuals from three simulations.

Each of the simulated data sets has  $418 \pm 1$  astrometric data points and  $142 \pm 1$  radial velocity measurements. The exact numbers vary due to the random variations of the sampling pattern. Given that our fits have 13 free parameters, the number of degrees of freedom is  $n_{\text{dof}} \approx 2 \times 418 + 142 - 13 = 965$ .

Figure 6 shows the distribution of reduced  $\chi^2$  together with the flag whether a given fit is acceptable or not. Clearly, the reduced  $\chi^2$  can be used as discriminator. The largest reduced  $\chi^2$  corresponding to a fit classified as ‘acceptable’ is 1.36, the smallest reduced  $\chi^2$  corresponding to a fit classified as ‘not acceptable’ is 1.12. The optimum cut is at a reduced  $\chi^2$  of 1.22, yielding as many good fits above as bad fits below the threshold. The total number of fits misclassified by this cut is 41. The total number of bad fits is 409 and corre-

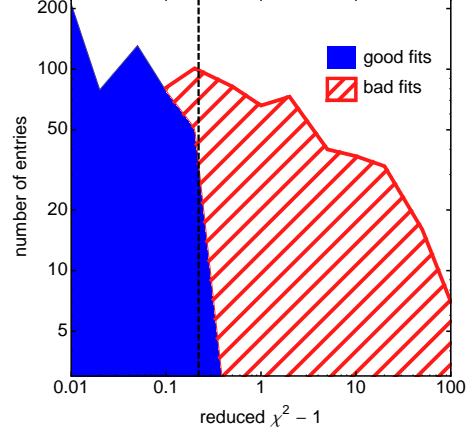


**Figure 6.** Distribution of reduced  $\chi^2$  for the 960 fits in logarithmic bins. Entries are coloured according to our visual classification of whether the residuals of any given fit is acceptable (blue/solid) or not (red/hatched). The black, dashed line marks the optimum cut at 1.22 separating good from bad fits by the value of their reduced  $\chi^2$ .

spondingly 551 fits have a reduced  $\chi^2$  below the threshold. Hence, the IBH would be detectable from the data in  $\approx 43\%$  of the cases. We find a dependence of the fraction of bad fits on the assumed mass for the IBH. For  $q = 10^{-4}$ ,  $2.5 \times 10^{-3}$ ,  $5 \times 10^{-3}$ ,  $10^{-3}$  the percentage of detectable IBHs is 15%, 39%, 51%, and 66%, respectively.

Having a reduced  $\chi^2 \geq 1.22$  corresponds formally to a  $4.7\sigma$  detection of the effects of the IBH for  $n_{\text{dof}} = 965$ . In reality, there will be perturbing effects such as confusion events, recognised or unrecognised. Hence, the actual  $\chi^2$  might be larger than in the simulations and the simple Gaussian statistics will not apply. We are nevertheless confident that by observing the astrometric (and photometric) residuals as a function of time the effects of an IBH can be disentangled from confusion events. The patterns of the residuals contain more information than a single  $\chi^2$  value.

In Figure 7 we examine the dependence of the reduced  $\chi^2$  on the black hole binary parameters. The left panel in the first row shows that the fits on average get worse when the mass of the assumed IBH is increased, as expected. The right panel in the first row shows that a value for the semi major axis of the IBH around  $\approx 1$  mpc leads on average to the worst fits. These two parameters correlate actually best with the reduced  $\chi^2$ , and in Figure 8 we show the reduced  $\chi^2$  in the  $M_{\text{IBH}}-a$ -plane. The unacceptable fits occupy a well-defined region in this plot.

The goodness of the fits, on the other hand, is fairly independent of the eccentricity of the IBH orbit (second row of Figure 7, left panel). The right panel in the second row shows that the periapsis distance  $p = a(1-e)$  of the IBH is a less good predictor for the fit than the semi major axis. The reduced  $\chi^2$  does not correlate with the finite set of orbital orientations probed, as shown in the third row, left panel of Figure 7. Here,  $\alpha$  represents the angle between the angular momentum vectors of S2 and the IBH at the start of the simulations. This incidentally argues against the possibility that the observed deviations are due to Kozai oscillations, since the mechanism requires large relative inclinations to oper-

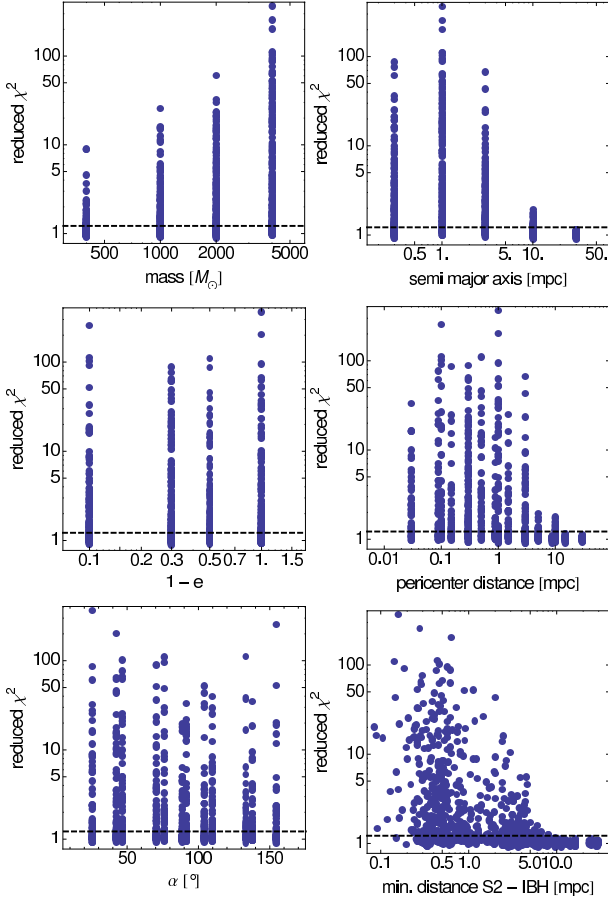


**Figure 7.** Distributions of reduced  $\chi^2$  for the 960 fits as a function of the black hole binary initial parameters: mass, semi-major axis, eccentricity, periape distance, orbital orientation and minimum distance to S2.

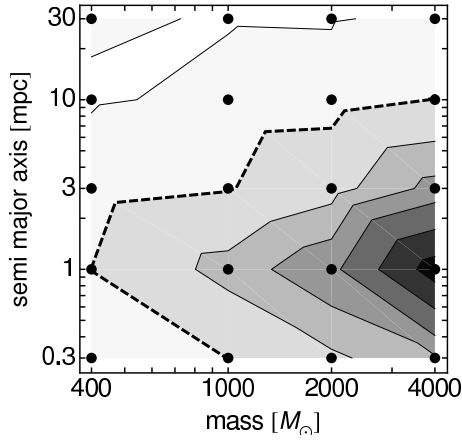


**Figure 8.** Reduced  $\chi^2$  for the 960 fits as a function of mass and semi major axis of the IBH. The plot shows the median at each grid point of the  $\chi^2$  values. The thick dashed line marks our threshold of  $\chi^2 = 1.22$ . Fits right of the line are not acceptable and thus the IBH would be discoverable.

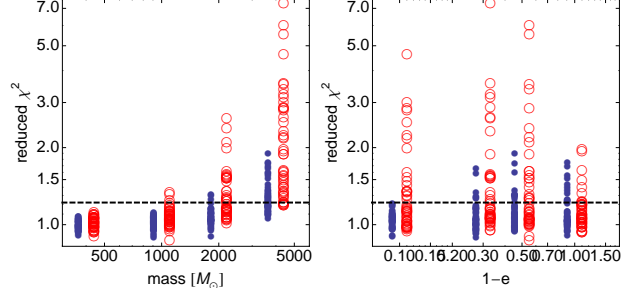


**Figure 9.** Reduced  $\chi^2$  as a function of black hole mass (left) and eccentricity (right) for two set of runs with the IBH starting at periaapsis (dots) and apoapsis (circles).

ate. However, fits with the same sets of parameters ( $q$ ,  $e$ ,  $a$ ) but different  $\alpha$  can have different values of  $\chi^2$ . This means that the knowledge of ( $q$ ,  $e$ ,  $a$ ) is insufficient to predict the reduced  $\chi^2$  but information on the sky position is necessary. Finally, the right panel in the third row of Figure 7 shows that the minimum 3D distance between S2 and the IBH also correlates with the reduced  $\chi^2$ . In general it holds that the smaller the minimum distance, the worse the corresponding fit. Clearly, this parameter is not independent of the semi-major axis.

The initial parameters adopted for the black hole binary are not sampled homogeneously. This is obvious for the first three panels in Figure 7 showing the reduced  $\chi^2$  as a function of the binary parameters ( $q$ ,  $e$ ,  $a$ ). But it also holds (and is less obvious) for the plot investigating the minimum distance between S2 and the IBH.

A comparison of the goodness of fit for the runs starting with the IBH at periaapsis and apoapsis is shown in Figure 9. In both cases, the semi-major axis of the black hole orbit is  $a = 10$  mpc. We find a modest worsening of the  $\chi^2$  in the case of an IBH initially at the apoapsis of its orbit. This can be attributed to the fact that S2's apoapsis, where the star spends most of its time, is about 10 mpc.

Finally, we also investigated the minimum time required for the IBH to become detectable. For this purpose, we repeated the orbital fits for a few cases assuming that the observations span 10, 15, 20, 25, 30, 35, 40, 45 or 50 years (Figure 10). Our initial conditions are such that the first periape passage of S2 happens after 10 years, the second after 26 years and the third after 42 years. Figure 10 shows that the reduced  $\chi^2$  starts to increase beyond our threshold of 1.22 after the second periaapsis passage for fits that show a large reduced  $\chi^2$  after 50 simulated years (red/dashed, blue/long-dashed and green/solid curves). Only for fits that after 50 simulated years have a reduced  $\chi^2 \lesssim 3$  is the threshold passed after the third periaapsis passage (black curve). The discrete nature of periape passages also is the reason why the blue/long-dashed and green/solid curves level out after about 45 years.

This is interesting in comparison with the current status of the observations. Since by now only one periape passage of S2 has been observed in 2002, one would not expect to have detected an IBH from the actual S2 data so far. This is particularly true since the assumed level of accuracy was not reached during the first years of the observations (1992 -

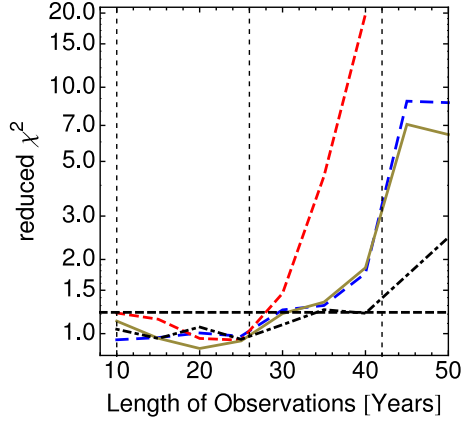


**Figure 10.** Reduced  $\chi^2$  as a function of the length of the observations for four cases: blue (long-dashed):  $q = 5 \times 10^{-4}$ ,  $e = 0.9$ ,  $a = 1$  mpc; red (dashed):  $q = 10^{-3}$ ,  $e = 0.9$ ,  $a = 1$  mpc; green (solid):  $q = 10^{-3}$ ,  $e = 0$ ,  $a = 0.3$  mpc; black (dot-dashed):  $q = 10^{-3}$ ,  $e = 0.7$ ,  $a = 3$  mpc. The vertical lines indicate the second and third periaapse passage covered by the simulations, the first one happens at  $t \approx 10$  yr. The horizontal, dashed line is our optimum cut at 1.22.

2002), and radial velocity information is only available after 2002 (with the exception of one point in 2000). Hence, the first real chance to detect an IBH will be after the next S2 periaapse passage, which will happen in 2018.

## 5 OTHER SOURCES OF ORBITAL TORQUE

Here we consider other perturbations that could induce changes in S2’s orbital angular momentum, potentially complicating the signal from an IBH. We find that almost all such alternative perturbations are small compared to the torque produced by an IBH.

Angles quoted in this section are intrinsic, not astrometric. As noted above, current data are able to determine the orbital angles  $(\varpi, \Omega, i)$  of S2 with an accuracy of about one degree. Changes induced by an IBH per orbit of S2 are  $10^{-3} \text{ deg} \lesssim \Delta(i, \Omega) \lesssim 1 \text{ deg}$  (Figure 2).

*Spin of the MBH.* Frame-dragging effects from a spinning MBH include an additional in-plane precession term as well as a precession of the orbital plane. Defining  $i'$  and  $\Omega'$  as the inclination and nodal angle of S2’s orbit with respect to the MBH’s equatorial plane, to lowest PN order, frame dragging induces changes

$$\Delta\varpi = -2A_J \cos i', \quad (14a)$$

$$\Delta\Omega' = A_J \quad (14b)$$

per revolution in the angle of periaapse and the line of nodes, respectively, where

$$A_J = \frac{4\pi\chi}{c^3} \left[ \frac{GM_{\text{MBH}}}{(1-e^2)a} \right]^{3/2} \quad (15a)$$

$$\approx 0.115' (1-e^2)^{-3/2} \chi \left( \frac{a}{\text{mpc}} \right)^{-3/2} \quad (15b)$$

and  $\chi \leq 1$  is the dimensionless spin of the MBH (e.g. Merritt et al. 2010). The orbital inclination  $i'$  remains unchanged. For S2, the spin contribution to advance of the

periaapse is  $\sim 1\%$  of the Schwarzschild contribution even for  $\chi = 1$  and so can be ignored. The nodal advance is  $\Delta\Omega' \approx 0.002 \chi \text{ deg}$ , too small to be detectable in the next few decades of monitoring, and smaller than the changes induced by an IBH in almost all of the runs carried out here (Fig. 2). Effects of frame dragging are only likely to be important for stars much closer to SgrA\* than S2 (Merritt et al. 2010). (Frame dragging could nevertheless be relevant to the orbit of an IBH. For the IBH orbit with smallest  $a$  (0.3 mpc) and largest  $e$  (0.9) considered here, the precession time drops to  $\sim 300\chi^{-1} \text{ yr.}$ )

*A stellar bar.* If the gravitational potential due to the distributed mass is appreciably non-spherical, the resultant torques could affect all of the orbital elements of S2 aside from  $a$ . For instance, the nuclear bar described by Alard (2001) has been modelled as a triaxial spheroid with central density  $\sim 150 \text{ M}_\odot \text{ pc}^{-3}$  (Rodríguez-Fernández & Combes 2008). In the most extreme case, the nuclear star cluster (NSC) of the Milky Way could be stratified on triaxial ellipsoids at all radii. A homogeneous, non-rotating triaxial bar induces changes in the inclination and nodal angle of a test star orbiting near the MBH, with characteristic time scale

$$T_{\Omega, i} \approx \frac{\sqrt{1-e^2}}{T_i - T_j} \frac{1}{PG\rho_b} \quad (16)$$

(Merritt & Vasiliev 2010, equations 11-15). Here,  $\rho_t$  is the density of the triaxial component, and  $(T_x, T_y, T_z)$  are the dimensionless coefficients, of order unity, that define the shape of the triaxial component (Chandrasekhar 1969); the torque in the  $(i, j)$  principal plane is proportional to  $T_i - T_j$ , etc. For S2, the angular reorientation over one orbit due to torques from a triaxial bar would be of order

$$\Delta\phi \approx 0.2 \text{ mas } (T_i - T_j) \left( \frac{\rho_b}{100 \text{ M}_\odot \text{ pc}^{-3}} \right), \quad (17)$$

undetectable even if  $\rho_b \approx 10^5 \text{ M}_\odot \text{ pc}^{-3}$ , the approximate density of the NSC at 1 pc from SgrA\*.

*Resonant relaxation:* Discreteness in the distribution of stars and stellar remnants is also a potential source of torque. “Vector resonant relaxation” produces changes in the direction of the orbital angular momentum of order

$$\Delta\phi \approx \frac{\sqrt{N}m}{M_{\text{MBH}}} \quad (18)$$

per radial period, where  $m$  is the mass of a background star and  $N$  is the number of such stars within S2’s orbit. Writing  $N = M_\star/m$ , with  $M_\star$  the distributed mass within S2’s orbit, this is

$$\Delta\phi \approx \left( \frac{M_\star}{M_{\text{MBH}}} \frac{m}{M_{\text{MBH}}} \right)^{1/2} \quad (19)$$

$$\approx 0.003 \text{ deg} \left( \frac{M_\star/M_{\text{MBH}}}{10^{-2}} \right)^{1/2} \left( \frac{M_{\text{MBH}}}{4 \times 10^6 m} \right)^{-1/2} \quad (20)$$

Since  $M_\star \lesssim 10^{-2} M_{\text{MBH}}$  (Gillessen et al. 2009), this is smaller even than the change due to frame-dragging unless the mean perturber mass  $m \gg M_\odot$ .

## 6 DISCUSSION AND CONCLUSIONS

We have shown that an IBH orbiting Sgr A\* at the distance of the S-stars can cause observable deviations in the orbit of

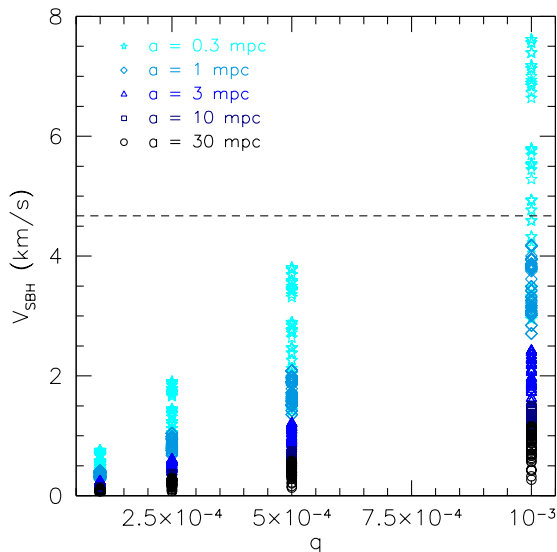


**Figure 11.** Root mean square velocity of the MBH as a function of the binary mass ratio. The dotted line represents the  $3\sigma$  limit on the 3D proper motion of SgrA\* derived from Reid et al. (2009).

star S2. The perturbations potentially affect all the orbital elements, but the key signature would be a change in S2's angular momentum (eccentricity, orbital plane) due to the non-spherically-symmetric forces from the IBH. In particular, we find that an IBH more massive than  $\sim 1000 M_{\odot}$  at a distance of  $\sim 1 - 5$  mpc is potentially discoverable at the next periastron passage of S2.

The presence of an IBH companion to the MBH might produce an observable feature in the radio observations of SgrA\*. In particular, some combinations of the binary parameters considered here might produce a reflex motion of the MBH which is larger than the currently available limits on the proper motion of SgrA\*. Such combinations of parameters could therefore be considered unlikely. Reid et al. (2009) report a proper motion of  $(7.2 \pm 8.5) \text{ km s}^{-1}$  in the plane of the Galaxy and of  $(-0.4 \pm 0.9) \text{ km s}^{-1}$  in the direction perpendicular to the plane. Since it appears unlikely that the motion of the MBH lies primarily in the Galactic plane, we adopt the value of the perpendicular component of the velocity as our fiducial value. In Figure 11 we compare the 3D root mean square velocity of the MBH obtained from the simulations with the observational  $3\sigma$  upper limit. We find that the motion of the MBH induced by the orbiting IBH is generally smaller than the  $3\sigma$  limit derived from radio observations of SgrA\*. Only for  $q > 10^{-3}$  and  $a = 0.3 \text{ mpc}$  does the simulated motion exceed the limit. Of course, if the motion induced by the IBH were to lie primarily in the Galactic plane, it would be very hard to detect via radio observations, even for large values of  $q$ .

## ACKNOWLEDGMENTS

DM acknowledges support from the National Science Foundation under grants no. AST 08-07910, 08-21141 and by the

National Aeronautics and Space Administration under grant no. NNX-07AH15G.

## REFERENCES

- Alard C., 2001, A&A, 379, L44
- Angélil R., Saha P., 2010, ApJ, 711, 157
- Chandrasekhar S., 1969, Ellipsoidal figures of equilibrium
- Eisenhauer, F., et al. 2005, ApJ, 628, 246
- Eisenhauer, F., et al. 2008, in Society of Photo-Optical Instrumentation Engineers (SPIE) Conference Series Vol. 7013 of Society of Photo-Optical Instrumentation Engineers (SPIE) Conference Series, GRAVITY: getting to the event horizon of Sgr A\*
- Fritz T., Gillessen S., Trippe S., Ott T., Bartko H., Pfuhl O., Dodds-Eden K., Davies R., Eisenhauer F., Genzel R., 2010, MNRAS, 401, 1177
- Fujii, M. et al. 2009, ApJ, 695, 1421
- . 2010, arXiv:1003.4125
- Genzel R., Schödel R., Ott T., Eisenhauer F., Hofmann R., Lehnert M., Eckart A., Alexander T., Sternberg A., Lenzen R., Clénet Y., Lacombe F., Rouan D., Renzini A., Tacconi-Garman L. E., 2003, ApJ, 594, 812
- Gerhard O., 2001, ApJL, 546, L39
- Ghez A. M., Duchêne G., Matthews K., Hornstein S. D., Tanner A., Larkin J., Morris M., Becklin E. E., Salim S., Kremenek T., Thompson D., Soifer B. T., Neugebauer G., McLean I., 2003, ApJL, 586, L127
- Gillessen S., Eisenhauer F., Fritz T. K., Bartko H., Dodds-Eden K., Pfuhl O., Ott T., Genzel R., 2009, ApJL, 707, L114
- Gillessen S., Eisenhauer F., Trippe S., Alexander T., Genzel R., Martins F., Ott T., 2009, ApJ, 692, 1075
- Gould A., Quillen A. C., 2003, ApJ, 592, 935
- Gualandris A., Merritt D., 2009, ApJ, 705, 361
- Hansen B. M. S., Milosavljević M., 2003, ApJL, 593, L77
- Kim S. S., Figer D. F., Morris M., 2004, ApJL, 607, L123
- Kinoshita H., Nakai H., 2007, Celestial Mechanics and Dynamical Astronomy, 98, 67
- Kozai, Y. 1962, AJ, 67, 591
- Levin Y., Wu A., Thommes E., 2005, ApJ, 635, 341
- Löckmann U., Baumgardt H., Kroupa P., 2009, MNRAS, 398, 429
- Madigan A., Levin Y., Hopman C., 2009, ApJL, 697, L44
- Martins F., Gillessen S., Eisenhauer F., Genzel R., Ott T., Trippe S., 2008, ApJL, 672, L119
- Merritt D., Alexander T., Mikkola S., Will C. M., 2010, Phys.Rev.D., 81, 062002
- Merritt D., Gualandris A., Mikkola S., 2009, ApJL, 693, L35
- Merritt D., Vasiliev E., 2010, ArXiv e-prints
- Mikkola S., Aarseth S. J., 1993, Celestial Mechanics and Dynamical Astronomy, 57, 439
- Mikkola S., Merritt D., 2008, AJ, 135, 2398
- Paumard T., Genzel R., Martins F., Nayakshin S., Beloborodov A. M., Levin Y., Trippe S., Eisenhauer F., Ott T., Gillessen S., Abuter R., Cuadra J., Alexander T., Sternberg A., 2006, ApJ, 643, 1011
- Perets H. B., Gualandris A., 2010, ArXiv e-prints
- Perets H. B., Gualandris A., Kupi G., Merritt D., Alexander T., 2009, ArXiv e-prints

- Perets H. B., Hopman C., Alexander T., 2007, *ApJ*, 656, 709
- Pott, J., et al. 2008, ArXiv e-prints
- Reid M. J., Menten K. M., Zheng X. W., Brunthaler A., Moscadelli L., Xu Y., Zhang B., Sato M., Honma M., Hirota T., Hachisuka K., Choi Y. K., Moellenbrock G. A., Bartkiewicz A., 2009, *ApJ*, 700, 137
- Rodriguez-Fernandez N. J., Combes F., 2008, *A&A*, 489, 115
- Rubilar G. F., Eckart A., 2001, *A&A*, 374, 95
- Schödel, R., et al. 2002, *Nature*, 419, 694
- Soffel M. H., 1989, *Relativity in Astrometry, Celestial Mechanics and Geodesy*
- Weinberg S., 1972, *Gravitation and Cosmology: Principles and Applications of the General Theory of Relativity*. Gravitation and Cosmology: Principles and Applications of the General Theory of Relativity, by Steven Weinberg, pp. 688. ISBN 0-471-92567-5. Wiley-VCH , July 1972.
- Zucker S., Alexander T., Gillessen S., Eisenhauer F., Genzel R., 2006, *ApJL*, 639, L21